Materials Research. 2022; 25:e20210629
DOI: https://doi.org/10.1590/1980-5373-MR-2021-0629

Influence of Welding Parameters on the Mechanical Properties and Microstructure of 7075-T651 Aluminum Alloys Welded Joints Performed by FSW Process

***Jefferson Segundo de Lima*[a,b]*, *Oclávio Coutinho dos Santos*[b], *Antônio Almeida Silva*[b], *Raphael Henrique Falcão de Melo*[b,c], *Theophilo Moura Maciel*[b]**

[a]*Universidade Federal de Pernambuco, Departamento de Engenharia Mecânica, Recife, PE, Brasil.*
[b]*Universidade Federal de Campina Grande, Engenharia Mecânica, Campina Grande, PB, Brasil,*
[c]*Instituto Federal de Educação Ciência e Tecnologia da Paraíba, Itabaiana, PB, Brasil.*

Received: December 28, 2021; Revised: May 30, 2022; Accepted: August 01, 2022

Aluminum alloys of 7xxx series have excellent characteristics and mechanical properties, being widely used in primary aircraft structures. However, the welding of these alloys by conventional arc welding processes results in an excessive mechanical resistance degradation and increasing in residual stress level. In this context, Friction Stir Welding (FSW) process has received attention in recent years mainly because it does not reach the materials melting point during the process. This work aims to evaluate the influence of the tool rotation and welding speed on microstructure and mechanical properties of AA 7075-T651 aluminum alloy welded joints by FSW process. Therefore, four welded joints obtained with different welding and tool rotation speed were subjected to tensile and microhardness tests. The microstructures of the welded joints were evaluated through analysis by optical microscopy and Scanning Electron Microscopy (SEM). The retreating side of the welded joints showed a higher occurrence of microstructural welding defects. Welded joints with yield strength (YS) 50% higher than those of base metal and with ultimate tensile strength up to 380 MPa were achieved.

Keywords: *Welded joint, Friction Stir Welding, 7075-T651 Aluminum Alloy, Microstructure, Mechanical properties.*

1. Introduction

The usage of aluminum has experienced a steady growth in several industry sectors. The combination of low density, high corrosion resistance, good hardness, excellent formability and recyclability guarantee its use on an industrial scale. Furthermore, aluminum can be combined with a wide range of other alloying elements, further expanding its applicability[1].

Among the different types of aluminum alloys, Al - Zn alloys (7xxx series) are the most used in the aeronautical industry, as they offer a high mechanical strength/weight ratio[2,3]. However, welding of this type of aluminum alloy by conventional fusion processes requires a series of precautions in order to avoid the loss of mechanical properties due to the solubilization and coalescence of precipitates, formation of coarse solidification structures, distortion and high level of residual stresses, among other solidification defects[4-6]. To overcome such issues imposed by traditional welding processes, the application of the friction welding process in which the union of parts occurs without fusion has been used more intensively[7,8].

Developed and patented by The Welding Institute, UK, in 1991, the Friction Stir Welding (FSW) process consists of a rotating tool of high mechanical strength with a specific profile, which is inserted into the material, advancing continuously, generating heat and promoting a mechanical mixing of the metals involved, making a high quality welded joint without the need of filler metal[9]. However, the FSW process has several variables that can influence the performance of the weld joint, such as tool rotation speed, tool geometry, travel speed, tool rake angle, axial force, and tool shoulder penetration. Therefore, prospective studies has been done on the influence of these welding parameters on the mechanical properties of welded joints[10-12].

In this context, this paper aims to evaluate the influence of some parameters, such as travel speed and tool rotation speed of the FSW process, on the mechanical properties and microstructure of aluminum alloy AA7075-T651 welded joints.

2. Materials and Methods

In the context of this research, aluminum sheets of alloy 7075-T651 with dimensions of 6x60x120 mm were used. Table 1 shows the nominal chemical composition of the plates, according to the manufacturer.

To assess the influence of the variation in welding parameters on the welded joint mechanical properties and microstructure, four joints were performed using the FSW process, varying the travel speed and tool rotation speed, as shown in Table 2. The levels and variables selected for setting the design of experiments, and consequently to the welded joints manufacturing process, were extracted from the technical literature on the study of aluminum alloys 7075-T651welded joint by the FSW process[12,13], in function

*e-mail: jefferson.segundo@ufpe.br

Table 1. Nominal chemical composition of the AA7075-T651 alloy (%).

Zn	Mg	Cu	Cr	Al
5.6	2.5	1.6	0.23	Balance

Table 2. Welding parameter values used.

WELDING PARAMETER		Welded joint
Tool rotation speed [RPM]	Travel speed [mm/min]	
410	48	1
1415	48	2
410	118	3
1415	118	4

and adequacy to the values supported by the available machinery (milling machine).

The welding tool used has a shoulder diameter of 16 mm and a pin diameter of 6 mm, with a straight cylindrical geometry. The tool and its dimensions can be seen in Figure 1. For the tool manufacturing, it was used an H13 tool steel for hot work which, after machining, it was subjected to heating at 1050°C for 25 minutes and cooled to air, in order to obtain the hardness and wear resistance necessary for use in the welding process[14].

The joints welded by the FSW process were made on a universal milling machine, model FU-300, with adjustment of the travel speed, inclination and tool rotation speed. The tilt angle of the tool was kept at 3° throughout the entire process.

The support for fixing the plates, seen in Figure 2, prevents the separation of the weld faces during operation and restricts the vertical movement of the plates, ensuring an adequate placement for welding.

To determine the tensile strength of the joints, a universal testing machine, model MTS-810, was used. The dimensions of the specimens and procedures for tensile tests were in accordance with ASTM E8M[15] with a displacement rate of 1 mm/min until failure.

The metallographic samples were prepared according to the standard metallographic procedure, sanded, polished and etched with Keller's reagent (95 mL H2O, 2.5 mL HNO3, 1.5 mL HCl, 1.0 mL HF). Macro and microstructural analysis were performed by Optical Microscopy (OM), while Scanning Electron Microscopy (SEM) was used for tensile fracture analysis of welded samples and base metal.

Vickers hardness tests (HV) on all welded joints, applying a load of 200 gf for 15 seconds were performed using an specimen of 1 mm between the indentations along a horizontal line passing by the base metal (BM), heat-affected zone (HAZ), thermo-mechanically affected zone (TMAZ) and stir zone (SZ)[16] as illustrated in Figure 3.

The indentations were performed using a FutureTech FM-700 digital microhardness tester.

3. Results and Discussions

3.1. Visual inspection

The visual appearance of the joints can be seen in Figure 4. No defects such as tunnels or cracks along the surface of the weld beads were identified, indicating good adequacy of the tool inclination angle of 3° in relation to the superficial quality of the welded joints.

The welded joint 1, Figure 4a, does not show any type of apparent surface defect. However, welded joints 2 and 4, Figure 4b and Figure 3d respectively, present coarse burr generation, due to the higher rotation speed value of the tool used in their manufacturing. Still in welded joint 4, there is a small crack at the tool exit point. The welded joint 3, Figure 4c, is characterized by an irregular weld bead with an excess of fine burr.

The advance side (AS) is at the top of the weld beads in Figure 4, while the retreating side (RS) is at the bottom. The concentration of burr produced during the FSW

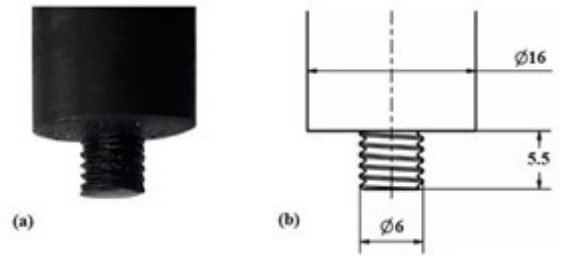

Figure 1. FSW tool: (a) manufactured and (b) design dimensions (in 'mm').

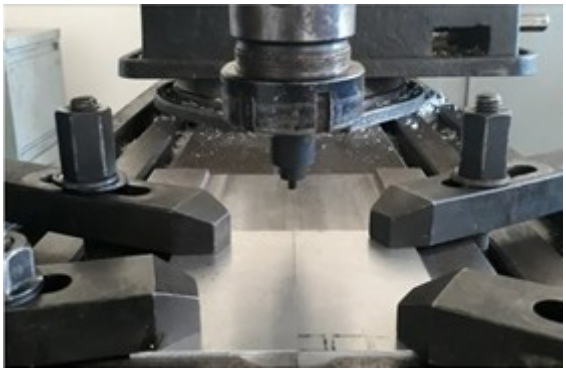

Figure 2. Fixing plates for welding execution.

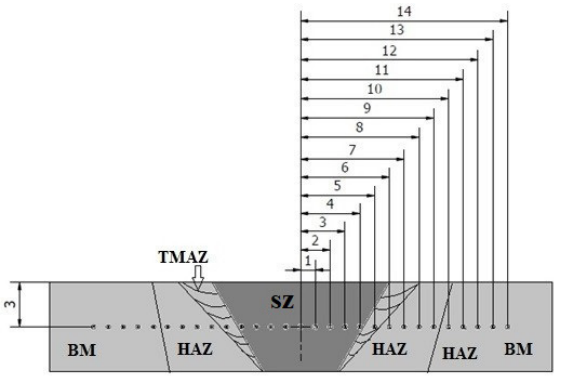

Figure 3. Representation of the distribution of microhardness indentations (dimensions in 'mm').

welding process is checked to the RS on the surface of the weld joints. Since the material flow in the AS and the RS is different[17], it suggests that the burr presence on the RS is due to the greater material transport from the AS to the RS by the tool during the welding process, which may indicate the presence of internal defects in the welded joints linked to the lack of material, in the location corresponding to the Cavaliere et al.[18] reported that welding different series of heat-treatable aluminum alloys showed that the accumulated material (in the form of burr) in the tool RS strongly influences the material mixture during the FSW process.

3.2. Macro and microstructure

The microstructure of AA 7075-T651 aluminum sheets as received is presented in Figure 5. It can be seen elongated grains in the rolling direction, with the presence of a reasonable number of precipitates and insoluble intermetallic particles in the matrix identified as small black dots, as reported by Lotfi and Nourouzi[13] when studying the corresponding series aluminum alloy.

Figures 6-9 show cross sections of the welded joints with the different welding parameters.

Figure 6a reveals the grain morphology in the different weld regions of welded joint 1. The morphology of elongated and deformed TMAZ grains bordering the SZ is observed in Figure 6b. Note that the resulting microstructure in the weld core, SZ in Figure 6c, has refined grains with homogeneous distribution when compared to the other analyzed weld regions. This is due to the intense mechanical work that the FSW process exerts on the aluminum sheets during the joining process. On the other hand, Figure 6d reveals the transition region from HAZ to BM with a tendency of elongation and narrowing of the grains towards BM, denoted by the colors darkening.

The presence of "onion rings", Figures 6a and 6c, is verified in the region corresponding to the weld nugget, inside the SZ. Onion rings marks the material transport phenomena that occur during the process. The circular movement induced by the tool leads to concentric circles that are distinct from each other by reducing the characteristic radius of each one, forming layers similar to onion rings, indicating the mixture between the materials in the SZ[19].

The grain morphology of the cross section of welded joint 2, Figure 7a, reveals a larger area of the TMAZ, characterized by a greater number of elongated and deformed grains close to the SZ, clearly observed in Figure 7b and 7d.

OM analysis of welded joint 2 reveals welding defects such as wormhole, Figure 6c, due to lack of mixing and filling material. It is important to emphasize the location and positions of these defects, since the friction welding process acts differently in the different regions of the welded joint, with the defects located on the tool recoil side.

The deformed and elongated grain regions of the TMAZ in weld joint 3 are more limited than in welded joint 2, similar to that observed in weld joint 1. The boundary between TMAZ and SZ of weld joint 3 is observed in Figure 8b. The OM of welded joint 3 also reveals a wormhole defect, Figure 9c, in addition to a crack-like bond defect known as a

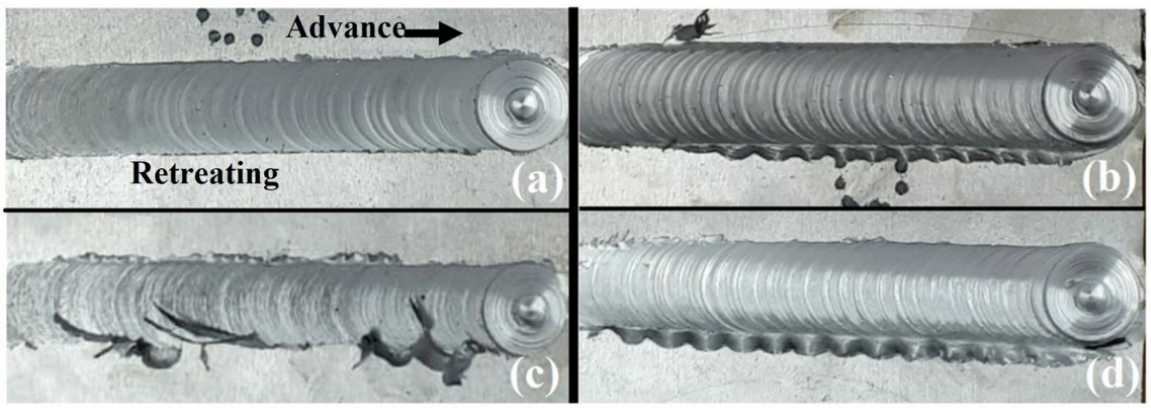

Figure 4. Visual appearance of the welds obtained by FSW: (a) welded joint 1, (b) welded joint 2, (c) welded joint 3, and (d) welded joint 4.

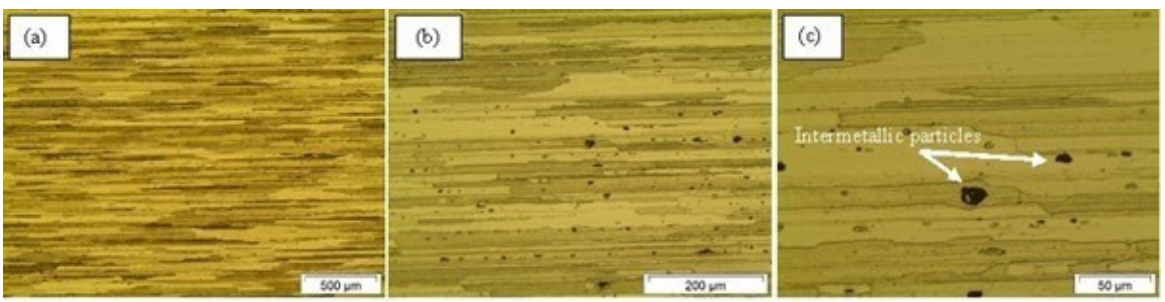

Figure 5. Observed microstructure of the AA 7075-T651 alloy, with magnifications of: a) 50x, b) 200x and c) 500x.

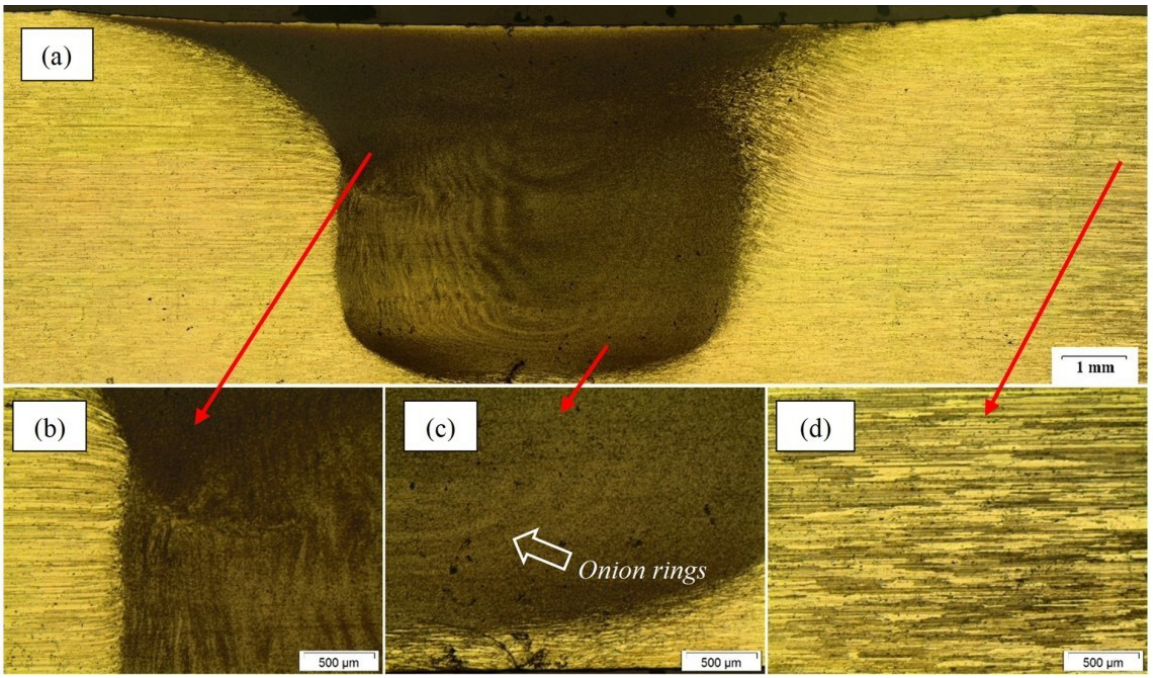

Figure 6. Macro and microstructure of welded joint 1: (a) Macrograph of the cross section, (b) Micrograph of the region between TMAZ and SZ, (c) SZ and onion rings, and (d) boundary between TMAZ and BM.

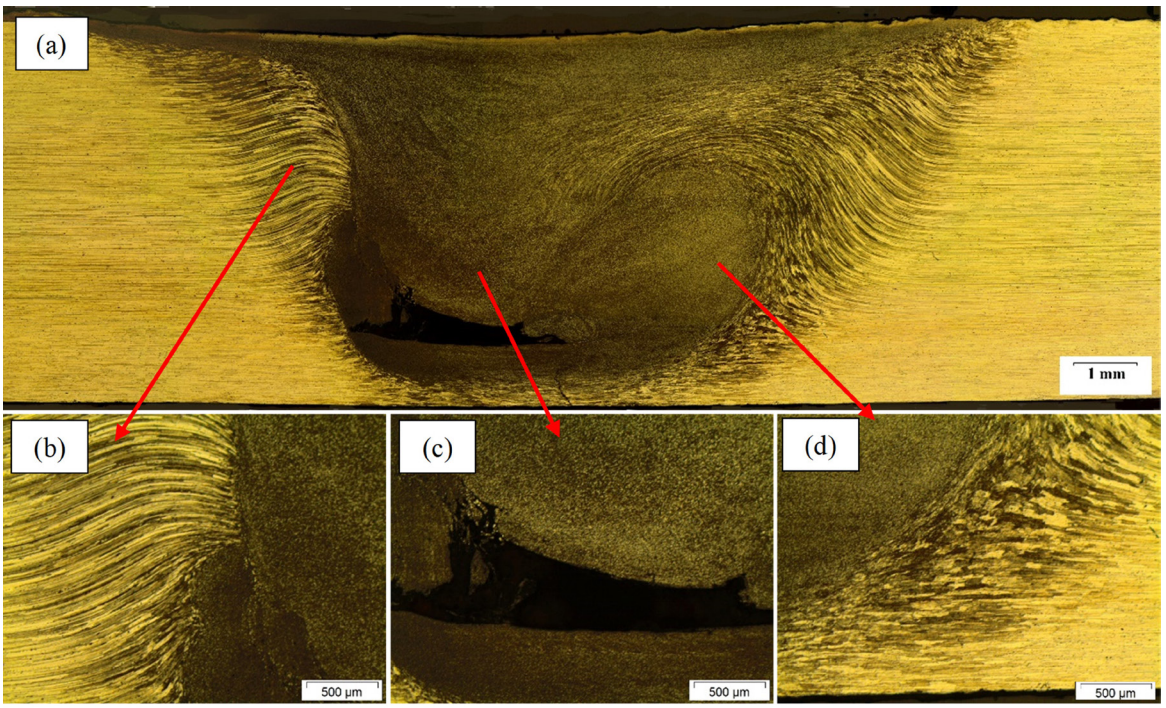

Figure 7. Macro and microstructure of the weld joint 2: (a) Macrograph of the cross section, (b) Micrograph of the region between TMAZ and SZ on the retreating side, (c) SZ and welding defect, and (d) boundary between SZ and TMAZ on the advance side.

"kissing bond", Figure 8d. As occurred in welded joint 2, the wormhole defect is located on the retreating side of the tool.

The OM of welded joint 4, Figure 9, reveals a variation of the wormhole defect, with the presence of a tunnel, Figure 9d, and an unsuccessful joint structure, characterized by a clump of broken and unmixed particles, Figure 9b. As occurred in welded joint 3, the kissing bond defect is also observed in welded joint 4, Figure 9c.

As in welded joint 2, the grain morphology of the cross section of welded joint 4, Figure 9a, reveals a larger

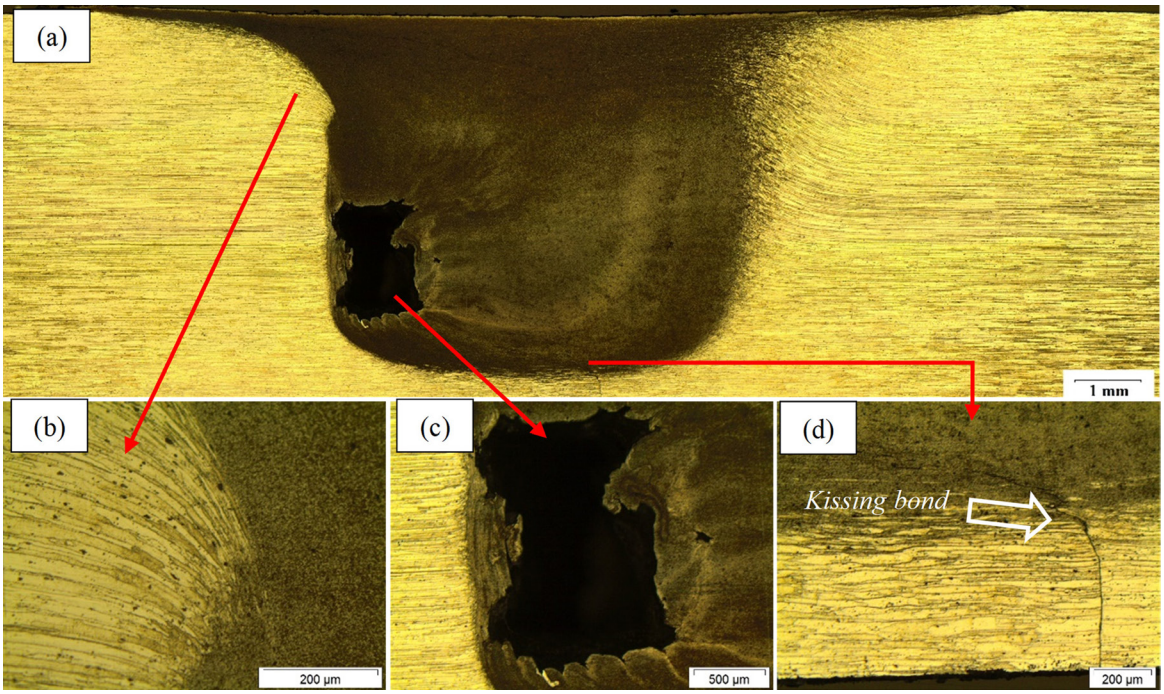

Figure 8. Macro and microstructure of the welded joint 3: (a) Macrograph of the cross section, (b) Micrograph of the region between TMAZ and SZ on the retreating side, (c) welding defect in the SZ on the retreating side, and (d) kissing bond welding defect.

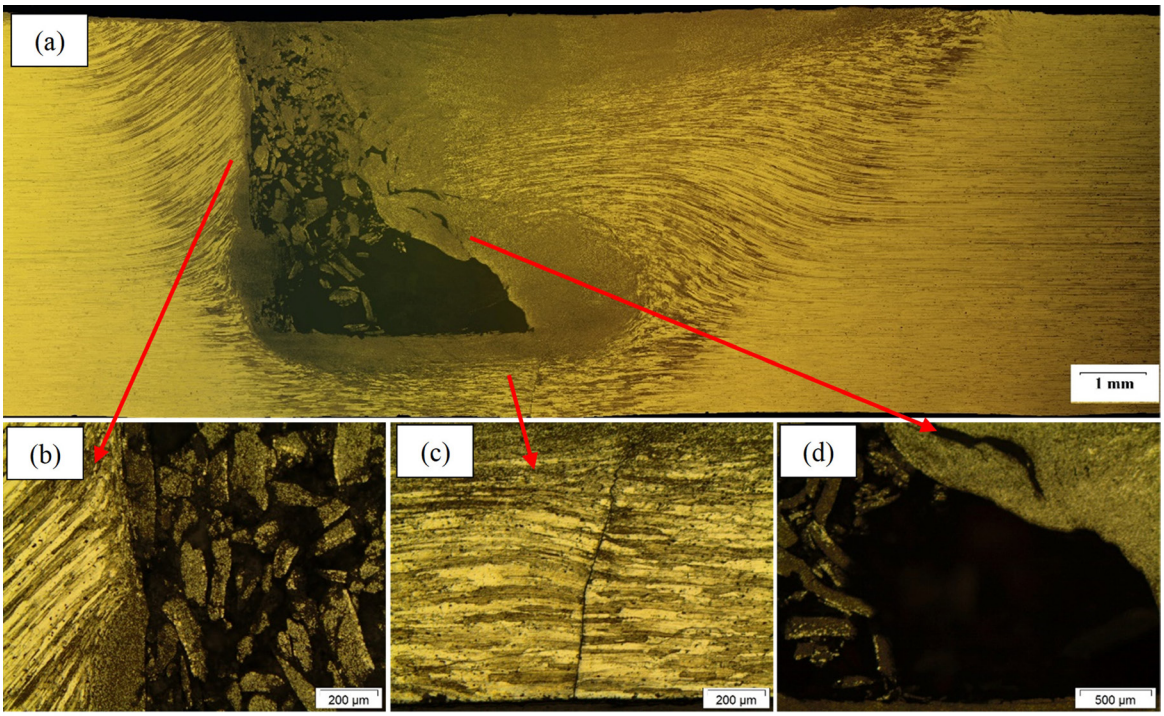

Figure 9. Macro and microstructure of the welded joint 4: (a) Macrograph of the cross section, (b) Micrograph of the region between TMAZ and SZ on the retreating side observing lack of mixture, (d) welding defect due to lack of union, and (c) welding defect in the SZ on the retreating side due to lack of mixture.

area of elongated and deformed grains at TMAZ, unlike to that observed in welded joints 1 and 3, Figures 6 and 7, respectively. These results indicates the influence of the tool rotation speed on the TMAZ extension and dimension. The greater rotation speed of the tool applied in the union of welded joints 2 and 4 caused greater mechanical work

on the welded plates, possibly generating greater heat input and mechanical deformation in the grains and, thus, a greater extension of the thermo-mechanically affected zone. The inverse is verified for welded joints 1 and 3 which have a more restricted area of the TMAZ. These results are similar to those obtained by Plaine et al.[20] in the welding of 304L stainless steel sheets by the FSW process with different tool rotation speeds.

The extent of deformed and elongated grains in the LA is significantly greater than those observed in the TMAZ RS similarly to that observed by Sharma et al.[21]. In AS, during welding, there is material traction in relation to the travel speed, while in RS there is a compression request with a shear component. The tensile deformation effect produces a well-defined region of the TMAZ-HAZ transition in the AS. This occurs due to the fact that the direction of the tool rotation speed is opposite to the travel speed in the AS, whereas both are the same in RS. The extent of deformation and the increase in the material temperature during mixing in AS are more severe than in RS[22].

Defects of lack of filling material by mixing, characterized by the presence of tunnels, are observed in welded joints 2, 3 and 4, located in the AS of the tool, indicating this region as a point of recurrence of these defects in aluminum joints welded by the FSW process. The combination of a welding speed of 48 mm/min and rotation speed of 410 RPM provided a welded joint with heat and sufficient material flow, providing an adequate mixture of materials, and consequently, preventing the formation of welding defects.

Although tool penetration was complete for welded joints 1 and 2, the presence of a kissing bond defect in welded joints 3 and 4 is noted near the root of the weld, as evidenced by the cross cuts made along the bead in Figures 8b and 9c. This may be related to the higher travel speed used when welding these joints, which causes less heat input during the union process[21]. As well as inadequate metal flow, hindering the mixing of materials and tool penetration, and the cylindrical geometry of the tool, causing the appearance of kissing bond defects[23]. A similar result was obtained by Kadlec et al.[24], in 7475-T7351 aluminum joints welded by FSW.

3.3. Microhardness profile

The Vickers microhardness profiles obtained from the FSW welded joints are shown in Figure 10.

Analyzing the microhardness profiles of welded joints 1 and 2, it is possible to observe a small increase in hardness at the center of the welded joints with a decrease in hardness near positions -8 mm and 8 mm, corresponding to the region of contact with the ends of the welding tool shoulder. The hardness values increase again and stabilize towards the BM, forming a hardness profile like the letter 'W'[25,26].

The increase in hardness at the center of the weld is attributed to the grain refining that takes place in the SZ caused by the dynamic recrystallization that occurred in the region, due to the intense mechanical work that the material undergoes during the friction welding process. The drop in hardness in the adjacent regions, TMAZ and HAZ, is probably due to the heating and mechanical work that the tool shoulder exerts on the welded material, causing grain growth and elongation with lower hardness compared to SZ and BM, according to the Hall-Petch relationship, which predicts greater mechanical strength in smaller grains[27]. Similar results were obtained by Rajakumar et al.[11], Sivaraj et al.[28] and Mohammadi-Pour et al.[29] for this same alloy welded by the FSW process.

Welded joints 3 and 4 do not show the same hardness profile observed in joints 1 and 2, possibly due to welding defects located close to the hardness verification regions, which considerably reduced the hardness values in the indented regions due to the presence of discontinuities and empty spaces. In welded joint 3, it is still possible to see a greater drop in hardness in the AS, region corresponding to HAZ and TMAZ.

In the hardness distribution of welded joint 4, there is a sharp drop in hardness values between positions -2 mm and -5 mm located in the AS of the tool, due to the presence of a discontinuity between the TMAZ and SZ, caused by inadequate mixing, possibly due to the combination of a higher travel speed and tool rotation speed, generating greater efforts for the tool movement, thus reducing the homogeneity of the plastification and mixture of the welded metal. The location coincides with the welding defect location seen in the macrograph of the welded joint, Figure 9a.

3.4. Tensile strength of welded joints

The stress-strain curves obtained in the uniaxial tensile tests can be seen in Figure 11. The welded joints had different tensile strength values. This difference can be explained by the presence of internal defects and by the change in heat input during each welded joint, generating zones with different widths in the weld region, and by the fluidity of the metal mixture, due to the interaction of the parameters used[30].

Welded joints 1 and 3, obtained with lower rotation speed, 410 RPM, showed better stress-strain behavior, reaching higher values of Yield Strength (YS), Tensile Strength (TS) and Deformation to Fracture (DEF). Meanwhile, welded joints 2 and 4, with the highest rotation speed of 1415 RPM, presented lower performance with a fragile fracture, and without plastic deformation. These results are consequence of the greater heat input generated during the process.

The increase in rotation speed led to a lower tensile strength, due to the greater heat input that leads to higher temperatures in the affected areas, increasing the effects of grain growth and precipitate dissolution[21,30].

The values of YS, TS and DEF can be better observed in Figure 12. It is possible to notice a reduction in YS and TS in relation to the BM, which are results already expected, due to the growth and elongation of grains in the HAZ[31].

The tool rotation speed of 410 RPM and travel speed of 48 mm/min ensured a TS of 380 MPa at joint 1 without the presence of internal welding defects, and it is the only acceptable performance among the combinations of parameters analyzed, superior to similar welded joints obtained by the arc welding process[32-34].

3.5. Fractography

Detailed fractographic analyzes using SEM on tensile fractured surfaces of the BM and welded joints 1 and 4 can be seen in Figure 13, at magnifications of 30X, 500X and 2000X.

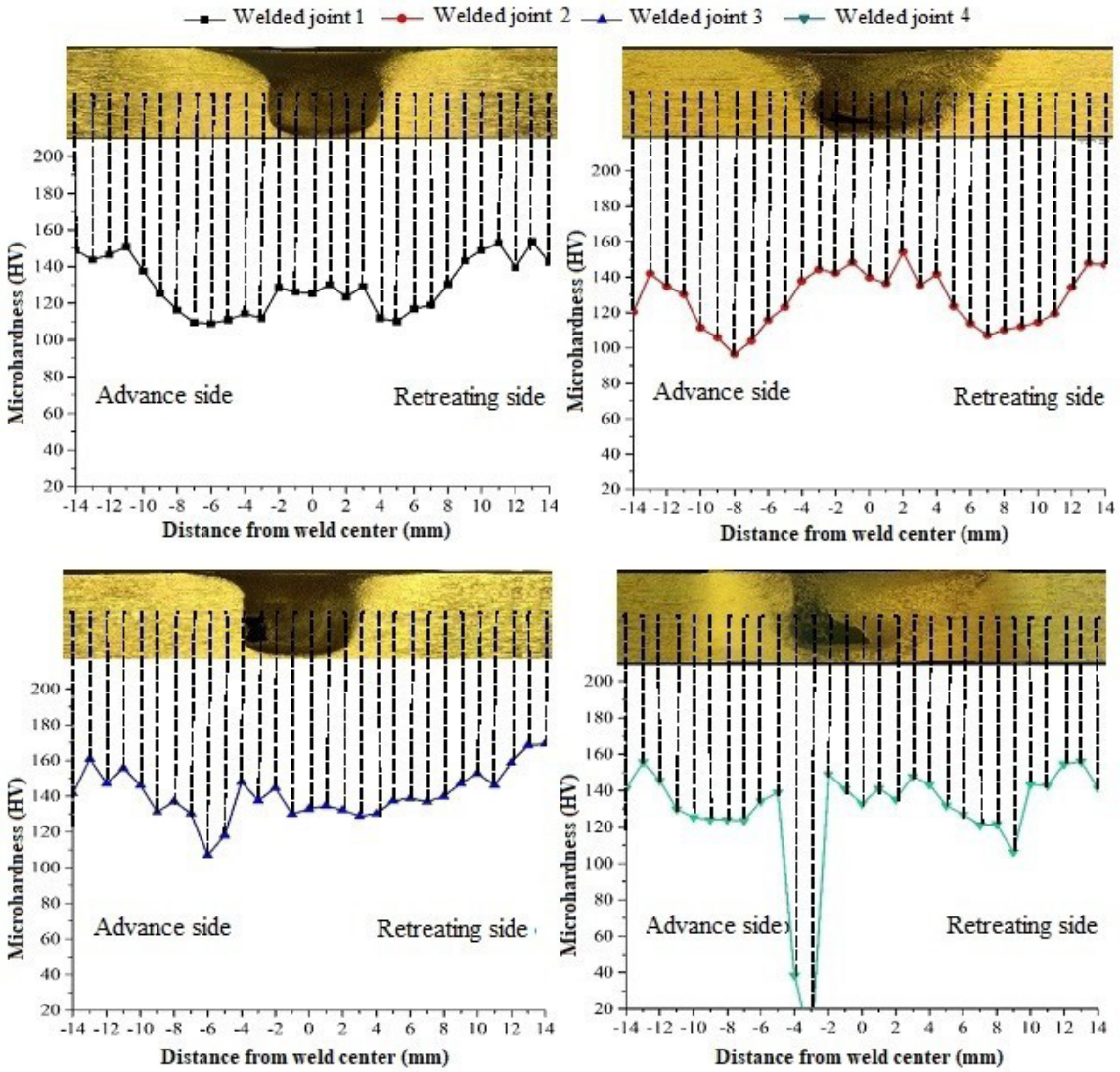

Figure 10. Hardness distribution in the cross section of welded joints.

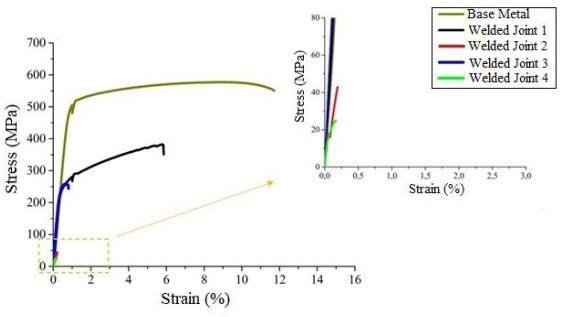

Figure 11. BM and welded joints stress-strain curves.

BM and welded joint 1, with a higher level of deformation and tensile strength, presented ductile fracture, with the presence of spherical microcavities (dimples), while welded joint 4, with less deformation and tensile strength, exhibited a fragile fracture.

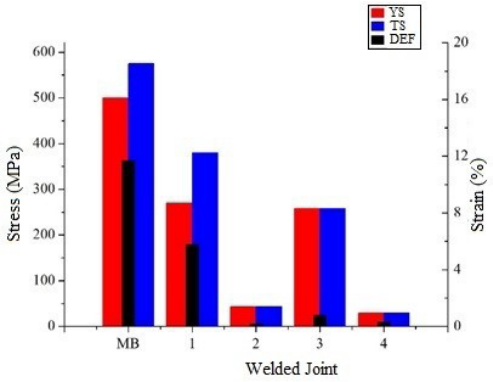

Figure 12. Main values obtained in the uniaxial traction test.

From the analysis, it was observed in welded joint 1 the presence of many cavities and absence of flat regions, showing extensive plastic deformation. This is characteristic of a ductile

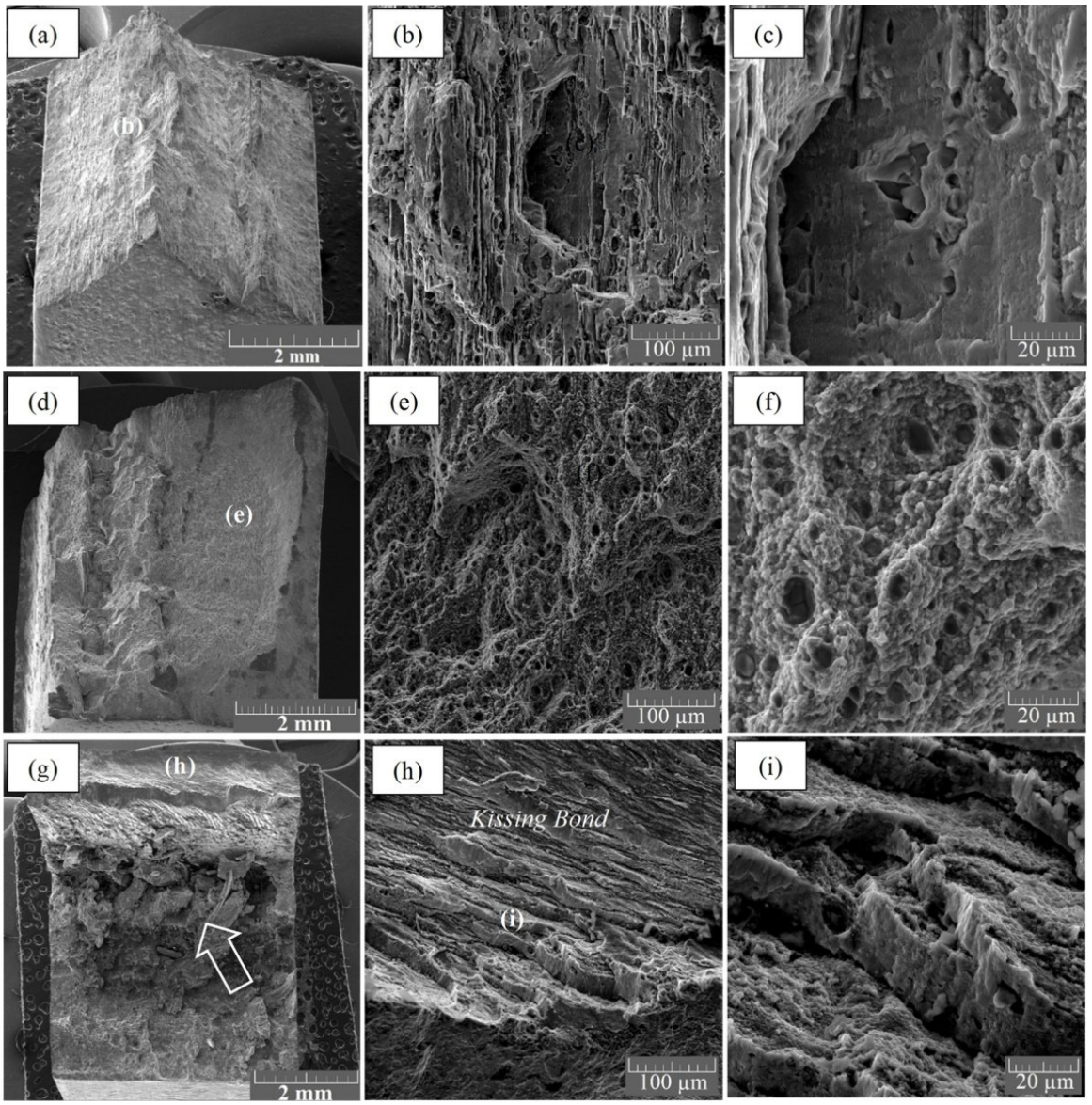

Figure 13. Fractographic analysis via SEM: (a) BM 30x, (b) BM 500x, (c) BM 2000x, (d) welded joint 1 in 30x, (e) welded joint 1 in 500x, (f) welded joint 1 in 2000x, (g) welded joint 4 in 30x, (h) welded joint 4 in 500x, (i) welded joint 4 in 2000x.

fracture due to the presence of dimples and an extremely irregular-looking surface. In the BM analysis, a surface with a little more regular appearance (Figure 13a) and less presence of dimples (Figure 13b and 13c) is observed when compared to the fracture of the welded joint1. However, BM withstands greater deformations before fracture than welded joint 1, probably due to changes in grain morphology and the generation of higher levels of residual stresses inherent in welding process.

In turn, the welded joint 4 showed a fragile fracture without the occurrence of appreciable plastic deformation and a higher crack propagation, characterized by the presence of cleavage facets. Also, it is noteworthy the presence of regions with fragments due to the lack of union, indicated by an arrow in Figure 13g, corroborating the macro-structural analyzes that indicated the presence of wormhole and kissing bond defects.

Welded joint 4 suffered catastrophic failure due to the large presence of welding defects, such as tunnels and kissing bond, which were marked at the beginning of the fracture, in Figure 12h. The defect region is one of the main failure starting points, even in welded joints subjected to fatigue tests with notch[24]. The following micromorphological characteristics were observed on the fracture surface: Absence of striation mechanisms in the fracture areas; Multiple cracks, starting in direction approximately perpendicular to the applied stress and producing a fracture surface with many flat regions perpendicular to the axis of tension, as seen in Figure 13h.

The fracture surface region of welded joint 8, Figure 13i, showed a transgranular fracture with faceted texture and flat

regions, due to crack propagation originating from defects of lack of mixture, through welded aluminum alloy grains.

4. Conclusions

Optical microscopy analysis of the cross-sections of the welded joints allowed the identification of internal welding defects, such as the formation of tunnels, predominantly on the tool advance side.

The tool rotation speed was verified as the main influence parameter on the thermo-mechanically affected zone dimensions.

The Vickers microhardness test of aluminum joints welded by FSW (1 and 2) revealed a profile with higher hardness values at the center of the welded joints.

For those with greater internal defects, a greater drop in hardness at advance side was observed.

The combination between lower tool rotation speed, 410 RPM, associated with lower travel speed, 48 mm/min, produced the best tensile-strain performance joint, with the yield strength above 50% of that of the base metal and a tensile strength up to 380 MPa and no apparent welding defects. On the other hand, using higher travel speed, 118 mm/min, and higher tool rotation speed, 1415 RPM, produced welded joints of low mechanical resistance, due to a higher incidence of welding defects in the AS of the tool.

Fractographic analyzes via Scanning Electron Microscopy revealed ductile fracture for the welded joint with greater tensile strength and the beginning of a fragile fracture along with the kissing bond defect, for the welded joint of lower strength. The kissing bond defect acted as a natural stress concentration point, promoting premature failure of the welded joints.

5. Acknowledgments

The authors thank PRPIPG of the Instituto Federal de Educação, Ciência e Tecnologia da Paraíba for the investment and scholarship, through INTERCONECTA 2019-2020. To the metallography, microscopy and mechanical properties characterization laboratories of the Unidade Acadêmica de Engenharia Mecânica (UAEM) of the Universidade Federal de Campina Grande and for the scholarship 285/18 granted by Fundação de Amparo à Pesquisa da Paraíba (FAPESQ).

6. References

1. Davis JR. Alloying: understanding the basics. Materials Park, OH: ASM International; 2001. p. 351-416.
2. Cavaliere P. Friction stir welding of Al alloys: analysis of processing parameters affecting mechanical behavior. Procedia CIRP. 2013;11:139-44.
3. Khan NZ, Siddiquee AN, Khan ZA, Mukhopadhyay AK. Mechanical and microstructural behavior of friction stir welded similar and dissimilar sheets of AA2219 and AA7475 aluminium alloys. J Alloys Compd. 2017;695:2902-8.
4. Lee CY, Lee WB, Yeon YM, Jung SB. The Joint characteristics of friction stir welded Mg-Zn-Y alloy. Mater Sci Forum. 2005;475–479:555-8.
5. Maggiolini E, Tovo R, Susmel L, James MN, Hattingh DG. Crack path and fracture analysis in FSW of small diameter 6082-T6 aluminium tubes under tension-torsion loading. Int J Fatigue. 2016;92:478-87.
6. Yang C, Ni DR, Xue P, Xiao BL, Wang W, Wang KS, et al. A comparative research on bobbin tool and conventional friction stir welding of Al-Mg-Si alloy plates. Mater Charact. 2018;145:20-8.
7. Capelari TV, Mazzaferro JAE. Avaliação da geometria de ferramenta e parâmetros do processo FSW na soldagem da liga de alumínio AA 5052. Soldag Insp. 2009;14(3):215-27.
8. Texier D, Atmani F, Bocher P, Nadeau F, Chen J, Zedan Y, et al. Fatigue performances of FSW and GMAW aluminum alloys welded joints: competition between microstructural and structural-contact-fretting crack initiation. Int J Fatigue. 2018;116:220-33.
9. Padhy GK, Wu CS, Gao S. Friction stir based welding and processing technologies - processes, parameters, microstructures and applications: a review. J Mater Sci Technol. 2018;34(1):1-38.
10. Ji P, Yang Z, Zhang J, Zheng L, Ji V, Klosek V. Residual stress distribution and microstructure in the friction stir weld of 7075 aluminum alloy. J Mater Sci. 2015;50(22):7262-70.
11. Rajakumar S, Muralidharan C, Balasubramanian V. Influence of friction stir welding process and tool parameters on strength properties of AA7075-T6 aluminium alloy joints. Mater Des. 2011;32(2):535-49.
12. Rajakumar S, Muralidharan C, Balasubramanian V. Optimization of the friction-stir-welding process and tool parameters to attain a maximum tensile strength of AA7075-T6 aluminium alloy. Manuf Eng. 2010;224(8):1175-91..
13. Lotfi AH, Nourouzi S. Predictions of the optimized friction stir welding process parameters for joining AA7075-T6 aluminum alloy using preheating system. Int J Adv Manuf Technol. 2014;73(9-12):1717-37.
14. Coutinho CB. Materiais metálicos para engenharia. Belo Horizonte: Ed. Fundação Christiano Ottoni; 1992. 405 p.
15. ASTM: American Society for Testing and Materials. ASTM E8: ASTM E8/E8M standard test methods for tension testing of metallic materials 1. Annu. B. ASTM Stand. 4 No. C, 1. West Conshohocken: ASTM; 2010.
16. Jata KV, Semiatin SL. Continuous dynamic recrystallization during friction stir welding of high strength aluminum alloys.. Scr Mater. 2000;43(8):743-9.
17. Zhang Z, Zhang H. Material behaviors and mechanical features in friction stir welding process. Int J Adv Manuf Technol. 2007;35(1-2):86-100.
18. Cavaliere P, Santis A, Panella F, Squillace A. Effect of welding parameters on mechanical and microstructural properties of dissimilar AA6082-AA2024 joints produced by friction stir welding. Mater Des. 2009;30(3):609-16.
19. Mishra RS, Ma ZY. Friction stir welding and processing. Mater Sci Eng Rep. 2005;50(1-2):1-78.
20. Plaine AH, Campanelli LC, Alcântara NG, Santos JF. Influence of energy input in friction stir welding on structure evolution and mechanical behaviour of 304 austenitic stainless steel. In: 67º ABM International Congress; 2012; Rio de Janeiro. Anais. São Paulo: ABM; 2012. p. 1442-7.
21. Sharma C, Dwivedi DK, Kumar P. Effect of welding parameters on microstructure and mechanical properties of friction stir welded joints of AA7039 aluminum alloy. Mater Des. 2012;36:379-90.
22. Zhang Z, Liu Y, Chen J. Effect of shoulder size on the temperature rise and the material deformation in friction stir welding. Int J Adv Manuf Technol. 2009;45(9-10):889-95.
23. Bayazid SM, Farhangi H, Ghahramani A. Effect of pin profile on defects of friction stir welded 7075 aluminum alloy. Procedia Mater. Sci. 2015;11:12-6.
24. Kadlec M, Ru˚žek R, Nováková L. Mechanical behaviour of AA 7475 friction stir welds with the kissing bond defect. Int J Fatigue. 2015;74:7-19.
25. da Silva AAM, Arruti E, Janeiro G, Aldanondo E, Alvarez P, Echeverria A. Material flow and mechanical behaviour of

dissimilar AA2024-T3 and AA7075-T6 aluminium alloys friction stir welds. Mater Des. 2011;32(4):2021-7.
26. Delijaicov S, Silva PAO, Resende HB, Batalha MHF. Effect of weld parameters on residual stress, hardness and microstructure of dissimilar AA2024-T3 and AA7475-T761 friction stir welded joints. Mater Res. 2018;21(6):e20180108.
27. Callister WD, Rethwisch DG. Materials science and engineering. New York: John Wiley & Sons; 2011.
28. Sivaraj P, Kanagarajan D, Balasubramanian V. Effect of post weld heat treatment on tensile properties and microstructure characteristics of friction stir welded armour grade AA7075-T651 aluminium alloy. Def. Technol. 2014;10(1):1-8. http://dx.doi.org/10.1016/j.dt.2014.01.004.
29. Mohammadi-Pour M, Khodabandeh A, Mohammadi-Pour S, Paidar M. Correction to: microstructure and mechanical properties of joints welded by friction-stir welding in aluminum alloy 7075-T6 plates for aerospace application. Rare Met. 2017. In press.
30. Lima JS, Santos OC, Melo RHF, Maciel TM. Influência dos parâmetros do processo de soldagem sobre a resistência à tração de juntas de alumínio aeronáutico soldadas pelo processo FSW. In: III Simpósio de Pós-graduação em Engenharia Mecânica da Universidade Federal de Campina Grandee: Coletânea de Artigos; 2020; Campina Grande. Anais. Campina Grande: UFCG; 2020. p. 1-7.
31. Sarsilmaz F. Relationship between micro-structure and mechanical properties of dissimilar aluminum alloy plates by friction stir welding. Therm Sci. 2018;22(Suppl. 1):55.
32. Sivashanmugam M, Jothi Shanmugam C, Kumar T, Sathishkumar M. Investigation of microstructure and mechanical properties of GTAW and GMAW joints on AA7075 aluminum alloy. In: Frontiers in Automobile and Mechanical Engineering; 2010; Chennai, India. Proceedings. New York: IEEE; 2010.
33. Olabode M, Kah P, Hiltunen E, Martikainen J. Effect of Al2O3 film on the mechanical properties of a welded high-strength (AW 7020) aluminium alloy. Proc Inst Mech Eng, B J Eng Manuf. 2016;230(11):2092-101.
34. Temmar M, Hadji M, Sahraoui T. Effect of post-weld aging treatment on mechanical properties of Tungsten Inert Gas welded low thickness 7075 aluminium alloy joints. Mater Des. 2011;32(6):3532-6.